Volume 61
Number 71
14 September 2025
Pages 13209–13490

# ChemComm

Chemical Communications

rsc.li/chemcomm

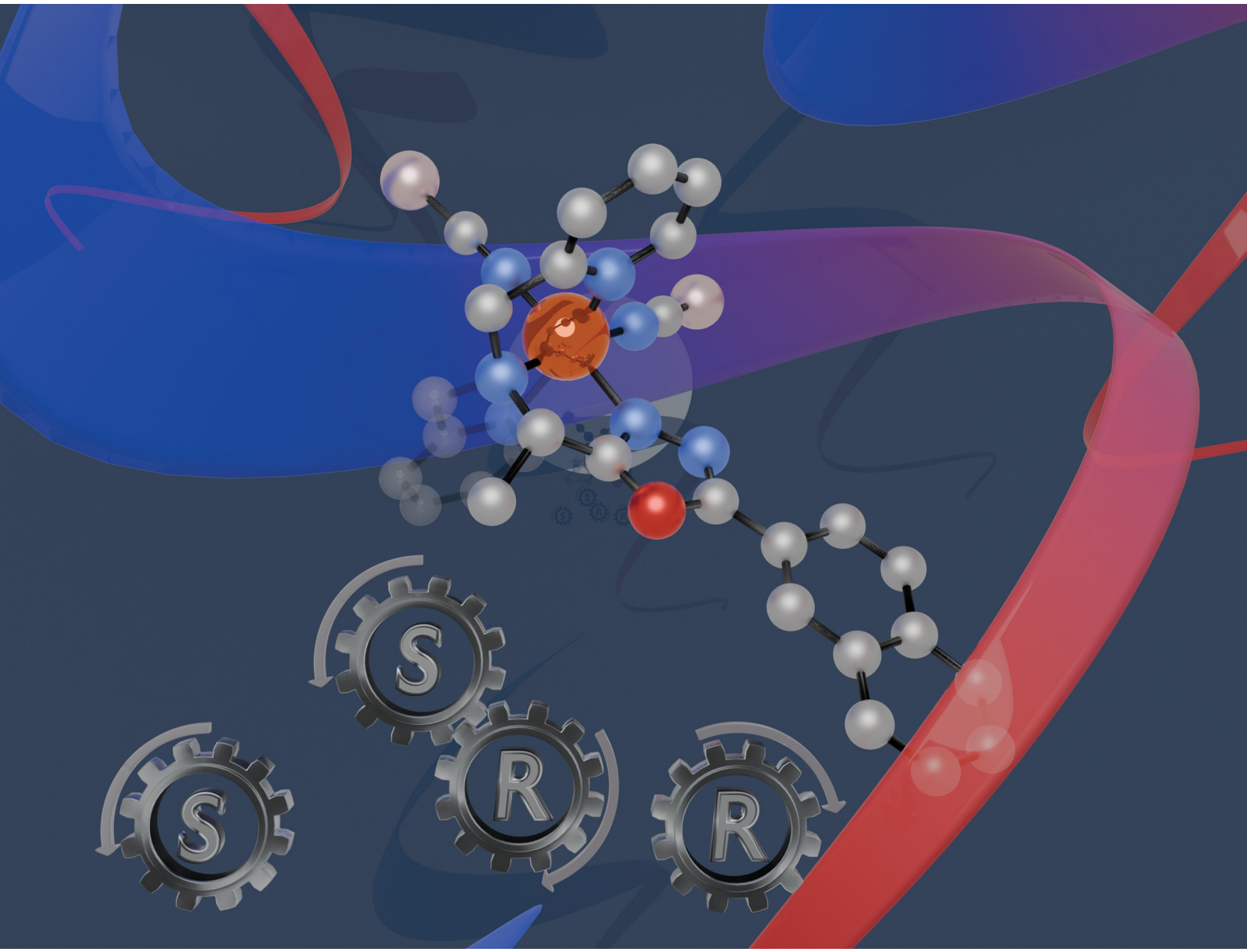


ISSN 1359-7345

ROYAL SOCIETY OF CHEMISTRY

**COMMUNICATION**

Eva Rentschler *et al.*

Chirality without compromise: identical spin crossover behavior between the racemate and the enantiopure Fe(II) complexes

ChemComm

COMMUNICATION

View Article Online
View Journal | View Issue



Cite this: *Chem. Commun.*, 2025, 61, 13389

Received 4th July 2025,
Accepted 24th July 2025

DOI: 10.1039/d5cc03779d

rsc.li/chemcomm



# Chirality without compromise: identical spin crossover behavior between the racemate and the enantiopure Fe(II) complexes†

Jens-Georg Becker, Sriram Sundaresan, Luca. M. Carrella and Eva Rentschler *

**The influence of chirality on the packing of solids, and consequently on the magnetic behavior of spin crossover (SCO) materials, is well documented. Here, we present an exceptional case involving three iron(II) complexes [Fe($L^{Naph\text{-}ODA\text{-}(X)\text{-}Al}$)($NCBH_3$)$_2$]·0.5 $CH_3CN$ (X = racemic (C1), *R* (C2), and *S* (C3)), based on a new 1,3,4-oxadiazole ligand ($L^{Naph\text{-}ODA\text{-}(X)\text{-}Al}$) with distinct stereocenters. These complexes have isostructural crystal lattices and identical incomplete thermal spin transitions with $T_{1/2} \approx 150$ K, but unexpectedly, single-crystal X-ray diffraction reveals that the presence and configuration of the stereocenters do not quantifiably impact the solid-state structure or the spin crossover properties.**

Molecular spin crossover (SCO) complexes have long been the subject of significant interest due to their potential application in memory devices, sensors and molecular switches, owing to their ability to reversibly switch between a low spin state (LS) and a high spin state (HS) in response to external stimuli, such as temperature, light, or pressure.[1,2] Chirality, on the other hand, serves as a powerful tool employed by nature both to store and to transmit information.[3] This is vividly illustrated by the helical structures of biomolecules such as DNA and proteins, whose specific handedness is critical to their biological functions. The chirality of these molecules encodes structural and functional information, guiding processes such as molecular recognition and replication. Recently, the convergence of these two phenomena in molecular materials opened avenues for the development of multifunctional materials, particularly for next-generation applications in spintronics, quantum sensing, and molecular logic, where spin and stereochemical control are key.[4,5]

Introducing a chiral element into a SCO active complex scaffold enables imparting enantioselective properties while, to the best of our knowledge, in all the cases known from the literature, this also modulates the magnetic behavior. Chirality can be introduced into SCO systems through chiral guests or anions,[6,7] spontaneous resolution,[8,9] supramolecular assembly,[10,11] or enantiopure ligands.[12–14] While ligand-based approaches offer precise stereochemical control, they are often limited by synthetic challenges and access to enantiopure precursors. It is well known from the literature that ligand chirality strongly influences coordination geometry, solid-state packing, and ultimately, the SCO behavior such as transition temperature, abruptness, and hysteresis.[12,15] All reported SCO systems with inbuilt chirality in the ligand backbone usually show an enantiomer dependent magnetic response because of the packing effects caused by the introduction of chiral substituents.[8,12]

A chirality independent spin switchable molecule enables these complexes to serve as experimental testbeds for a range of molecular spintronic phenomena, thereby providing a platform to investigate chiral-spin interactions in the absence of structural interference. In quantum devices dual encoding of the spin state and molecular handedness enables multi-level read/write operations within a single molecule.

Building on our previous work with asymmetric 1,3,4-oxadiazole ligands,[16–18] we now report a new synthetic strategy using chiral amino acids to access enantiopure ligands in fewer steps.

Both enantiomers *R*- and *S*-1-(5-(naphthalen-2-yl)-1,3,4-oxadiazol-2-yl)-*N*,*N*-bis(pyridin-2-ylmethyl)ethan-1-amine were synthesized enantiopure by a two-step synthesis procedure (Fig. 1), reacting the enantiopure amino acids *R*- and *S*-alanine with pyridinecarboxyaldehyde and sodium trisacetoxyborhydride in dichloromethane according to a literature known reductive amination.[19] The intermediate products bis(pyridin-2-ylmethyl)-*R*-alanine (I-*R*) and bis(pyridin-2-ylmethyl)-*S*-alanine (I-*S*) were obtained in moderate yields of 54% (I-*R*) and 30% (I-*S*) after purification by column chromatography. Both intermediate products were further reacted with carbonyldiimidazole as a coupling reagent in dry dichloromethane followed by nucleophilic

*Department Chemie, Johannes-Gutenberg-Universität Mainz, Duesbergweg 10–14, 55128 Mainz, Germany. E-mail: rentschl@uni-mainz.de*

† Electronic supplementary information (ESI) available: Experimental details, ligand and complex synthesis, and $^1$H-, $^{13}$C and 2D-NMR, IR, HRES-MS, UV-vis, PXRD, XRD and CD. CCDC 2467465–2467470. For ESI and crystallographic data in CIF or other electronic format see DOI: https://doi.org/10.1039/d5cc03779d

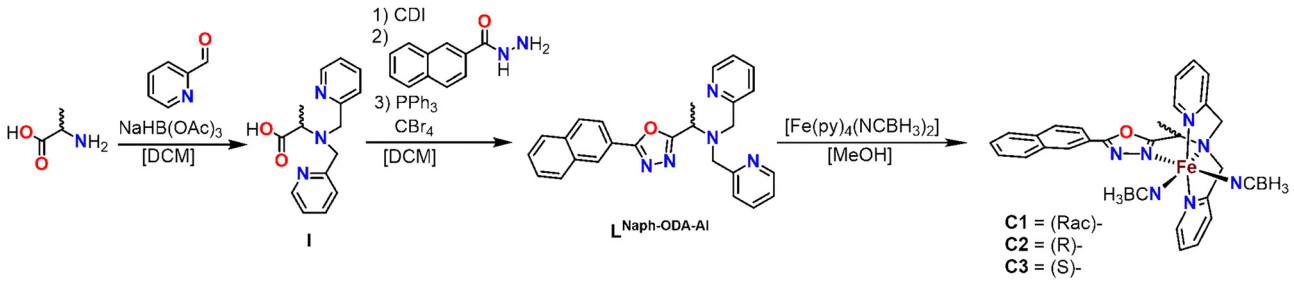


Fig. 1 Multistep ligand synthesis of $L^{Naph\text{-}ODA\text{-}(X)\text{-}Al}$ along with complex synthesis of [Fe($L^{Naph\text{-}ODA\text{-}(X)\text{-}Al}$)($NCBH_3$)$_2$]·0.5 $CH_3CN$ (**C1** X = *Rac*, **C2** X = *R* and **C3** X = *S*).

substitution with naphthohydrazide.[20] The dehydrative ring closure was successfully achieved by using carbon tetrabromide and triphenylphosphine in a one pot synthesis procedure.[20]

After purification by column chromatography both enantiopure products (*R*)-1-(5-(naphthalen-2-yl)-1,3,4-oxadiazol-2-yl)-*N*,*N*-bis(pyridin-2-ylmethyl)ethan-1-amine ($L^{Naph\text{-}ODA\text{-}(R)\text{-}Al}$) and (*S*)-1-(5-(naphthalen-2-yl)-1,3,4-oxadiazol-2-yl)-*N*,*N*-bis(pyridin-2-ylmethyl)ethan-1-amine ($L^{Naph\text{-}ODA\text{-}(S)\text{-}Al}$) were obtained in moderate yields of 67% ($L^{Naph\text{-}ODA\text{-}(R)\text{-}Al}$) and 35% ($L^{Naph\text{-}ODA\text{-}(S)\text{-}Al}$). Both the ligands, $L^{Naph\text{-}ODA\text{-}(R)\text{-}Al}$ and $L^{Naph\text{-}ODA\text{-}(S)\text{-}Al}$, were fully characterized by different analytical methods, including $^1$H-NMR-, $^{13}$C-NMR-, 2D-NMR-, IR-spectroscopy, and mass spectrometry. Chiral HPLC was employed to verify the enantiomeric purity of the ligands (Fig. S74 and S75, ESI†). The two ligands were used in a nitrogen atmosphere for complexation reactions with the known precursor [Fe(py)$_4$($NCBH_3$)$_2$] to obtain the three complexes [Fe($L^{Naph\text{-}ODA\text{-}(X)\text{-}Al}$)($NCBH_3$)$_2$]·0.5 $CH_3CN$ (**C1** X = *Rac*, **C2** X = *R*, and **C3** X = *S*) in moderate yields as powders (experimental details are in the ESI†). **C1** was obtained using a racemic mixture of the enantiopure ligands.[16] The bulk samples of the complexes were characterized by IR spectroscopy (Fig. S13–S17, ESI†),[21] ESI-MS (Fig. S18–S27, ESI†), and elemental analysis. Phase purity was verified using PXRD (Fig. S68–S70, ESI†). *R*- and *S*-chirality of the obtained complexes was confirmed by CD spectroscopy (Fig. S77, ESI†).

Single crystals suitable for X-ray diffraction (XRD) were obtained by recrystallization from acetonitrile. **C1** crystallizes in the monoclinic crystal system with the space group $P2_1/n$. In contrast, the enantiopure complexes **C2** and **C3** crystallize in the same monoclinic crystal system without the *n*-mirror plane, resulting in the chiral space group $P2_1$ (Tables S1–S6, ESI†). All complexes have identical unit cell sizes, parameters and the same molecule formula per unit cell ($Z$ = 4). The coordination sphere of the iron(II) centers is completed by two $NCBH_3$ co-ligands that occupy *cis* positions relative to each other. VT-SC-XRD studies reveal that the average Fe–N bond length at 90 K is 2.026 ± 0.010 Å, consistent with the intermediate or incomplete spin state. For comparison, a fully low spin (LS) configuration typically exhibits shorter Fe–N bonds, averaging around 1.97 Å.[16] The observed distortion parameters ($\Sigma$) range from 53.60° to 62.80° (± 3.63°). These values are notably higher than that of the reference low-spin complex [Fe($L^{Naph\text{-}ODA}$)($NCBH_3$)]·1.5 $CH_3OH$ $\Sigma_O(FeN_6)$ = 47.0°, confirming that all three complexes are in an incomplete low-spin state at low temperatures.[16]

SC-XRD measurements at 220 K reveal a spin state transition, as indicated by a significant increase in Fe–N bond lengths compared to 90 K. The average Fe–N bond length at 220 K is 2.167 ± 0.022 Å for all three complexes, consistent with a high-spin (HS) state.[16] This assignment is further supported by an increased octahedral distortion, with values ranging between $\Sigma_O(FeN_6)$ 85.90° and 92.41° ($\overline{\Sigma}_O(FeN_6)$ = 89.78 ± 3.30°).[22] These values are similar to those reported in the literature for [Fe($L^{Naph\text{-}ODA}$)($NCBH_3$)]·1.5 $CH_3OH$ ($\Sigma_O(FeN_6)$ = 94.0°; 2.17 Å), confirming the full transition to the high-spin state.[16] The spin transition is also confirmed by a 3.5% increase in the unit cell volume upon heating.

The enantiopure complexes **C2** and **C3** exhibit distinct point chirality due to the stereogenic methyl group, while the racemic complex **C1** features a distorted methyl group, indicating a random distribution of *R*- and *S*-enantiomers within the crystal lattice. In all three complexes **C1–C3**, the iron(II) center adopts a meridional coordination geometry with the ligand $L^{Naph\text{-}ODA\text{-}(X)\text{-}Al}$, which itself is achiral apart from the point chirality introduced by the methyl substitution, as previously noted.[16,23]

A possible facial coordination isomer would introduce chirality to the iron center, allowing for the formation of either the Λ- or Δ-isomers, by the positioning of the pyridine units, looking on the triangle area imparting $NCBH_3$, 1,3,4-oxadiazole unit and on pyridine unit (Fig. S78, ESI†). Λ- and Δ-isomers refer to the two possible chiral arrangements of octahedral metal complexes, where the ligands wrap around the metal center in left-handed (Λ) or right-handed (Δ) helicity. These stereoisomers may exhibit subtle differences in intermolecular packing and lattice interactions that influence the spin crossover properties (Fig. S78, ESI†).

Since the molecular structures of the complex units in **C1–C3** are similar, the impact of chirality on the packing should be considered. Investigation of the crystal structures along the *a*-axis reveals a consistent overall packing arrangement among the three complexes, as illustrated in Fig. 2. The only difference in packing arises from the orientation of the chiral methyl group. In all three complexes, the naphthyl groups from two complex units interact *via* π–π interactions, forming pairs. Similar interactions have been observed in related complexes.[16,24,25] Within the crystal lattice, the iron(II) centers of each pair are interlocked, with one $NCBH_3$ co-ligand pointing toward the adjacent complex. This interlocking arrangement results in a stair-like chain of pairs (Fig. S67, ESI†), further stabilized by interactions with neighboring pairs. Key π–π-stacking parameters, such as offset, normal vector,



 

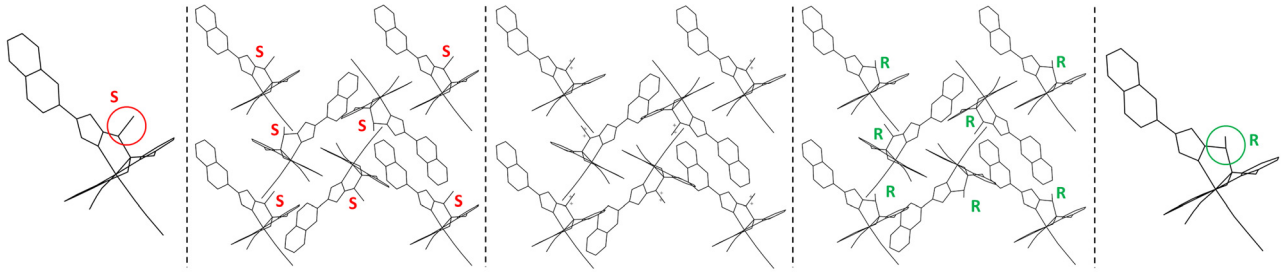


Fig. 2 Packing diagrams to visualize the similarities in the packing of the complexes [Fe($L^{Naph\text{-}ODA\text{-}(S)\text{-}Al}$)$(NCBH_3)_2$]·0.5 $CH_3CN$ (**C3**) (left), [Fe($L^{Naph\text{-}ODA\text{-}(Rac)\text{-}Al}$)$(NCBH_3)_2$]·0.5 $CH_3CN$ (**C1**) (middle) and [Fe($L^{Naph\text{-}ODA\text{-}(R)\text{-}Al}$)$(NCBH_3)_2$]·0.5 $CH_3CN$ (**C2**) (right). The methyl group is disordered in the case of the racemic mixture.

and centroid–centroid distances, were evaluated (Fig. S32, S37, S44, S49, S57 and S62 and Table S13, ESI†), revealing consistent values across the series. This structural similarity reflects the conserved packing motif among **C1–C3**. No significant hydrogen bonding interactions were identified using Mercury software package, emphasizing the dominant role of π–π interactions in directing the supramolecular architecture. Notably, these π–π contacts between naphthyl units are the primary contributors to the observed cooperativity.[16]

To the best of our knowledge, such an identical packing between racemate and enantiopure complexes has not previously been reported for chiral spin crossover complexes. In other cases, the introduction of the chiral centre alters the packing, which in turn usually changes the SCO behavior. This identical packing between the racemate and the enantiopure complexes presented here can be attributed to the minimal change in the ligand backbone caused be the introduction of a methyl group.

The temperature-dependent magnetic susceptibility behavior of all three complexes (**C1–C3**) was determined using pure microcrystalline samples from 10–300 K in both heating and cooling modes. A constant value of approximately 3.45 $cm^3$ K $mol^{-1}$ is observed for $\chi_M T$ at temperatures above 200 K for all complexes, confirming the high spin state concluded from single-crystal X-ray diffraction data. Upon decreasing the temperature, the $\chi_M T$ values decrease, showing a gradual spin-state transition with a $T_{1/2}$ = 150 K for all three complexes, leading to a plateau below 75 K with an average $\chi_M T$ value of 1.06 $cm^3$ K $mol^{-1}$ (Fig. 3). The gradual nature of the spin-state transition can be attributed to the presence of only weak or moderate interactions. The persistence of an incomplete spin transition below 75 K is likely due to solid-state packing constraints hindering full structural reorganization. This behavior may also result from a finely balanced ligand field environment that stabilizes a mixed-spin or intermediate spin state at low temperatures.[17] Further decreasing the temperature results in a drop in the magnetic moment below 10 K. This can be attributed to a combination of zero-field splitting and weak antiferromagnetic coupling effects between the complexes since π–π contacts of 3.4 Å are observed.

This work presents an unprecedented example of introducing chirality into spin-crossover (SCO) complexes *via* the chirality of an amino acid point, with no significant difference

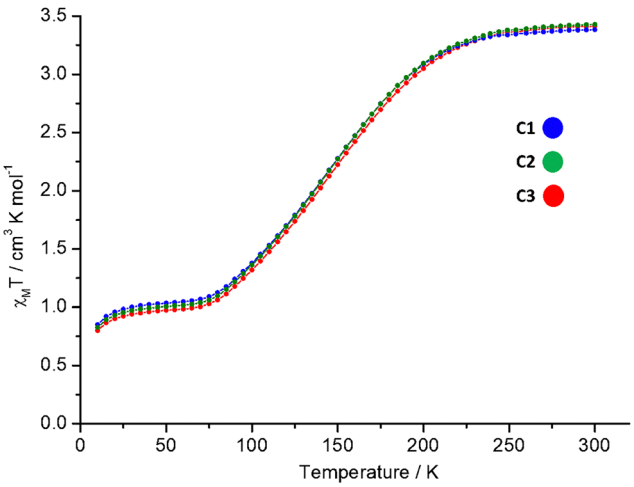


Fig. 3 $\chi_M$ *vs.* $T$ measured for powder products of [Fe($L^{Naph\text{-}ODA\text{-}(Rac)\text{-}Al}$)$(NCBH_3)_2$] (**C1**) (blue), [Fe($L^{Naph\text{-}ODA\text{-}(R)\text{-}Al}$)$(NCBH_3)_2$] (**C2**) (green) and [Fe($L^{Naph\text{-}ODA\text{-}(S)\text{-}Al}$)$(NCBH_3)_2$] (**C3**) (red) in the form of the resulting $\chi_M T$ *vs.* $T$ plot. Magnetic susceptibility was determined between 300 K and 10 K.

in packing between the racemic and enantiopure polymorphs. Identical powder X-ray diffraction (PXRD) patterns and a detailed structural analysis using single-crystal X-ray data confirm that all three complexes have the same crystal packing. This highlights the rare phenomenon of enantiomers sharing an identical packing motif and nearly identical SCO behavior. All complexes undergo a gradual, incomplete spin-state transition with a transition temperature ($T_{1/2}$) of 150 K.

Further investigations are underway to study the circular dichroism (CD)-light induced spin state transition (LIESST) phenomenon using polarized light in both racemic and enantiopure complexes. The goal is to elucidate the spin-selective photoresponse in this system. If successful, this system could be the first of its kind: a reversible optical handle for reading and writing spin states with chiral sensitivity.

The authors thank Dr Thomas and Prof. Besenius (JGU) for the CD spectral measurements and Mr Hagenow (JGU) for the evaluation of the CD data. JGB and ER acknowledge funding by the Deutsche Forschungsgemeinschaft (DFG, German Research Foundation) SFB TRR 173 Spin+X (268565370, project A04).

## Conflicts of interest

There are no conflicts to declare.

## Data availability

All the raw data from this manuscript have been uploaded to Zenodo and are freely available *via* the DOI: **https://doi.org/10.5281/zenodo.15798534**. All the processed data supporting the findings of this study can be found in the article and the ESI.†

## Notes and references

1 P. Gutlich, V. Ksenofontov and A. Gaspar, *Coord. Chem. Rev.*, 2005, **249**, 1811–1829.
2 J.-F. Létard, *J. Mater. Chem.*, 2006, **16**, 2550–2559.
3 Y. Liu, Z. Wu, D. W. Armstrong, H. Wolosker and Y. Zheng, *Nat. Rev. Chem.*, 2023, **7**, 355–373.
4 S. Ohkoshi, S. Takano, K. Imoto, M. Yoshikiyo, A. Namai and H. Tokoro, *Nat. Photonics*, 2014, **8**, 65–71.
5 W.-K. Han, L.-F. Qin, C.-Y. Pang, C.-K. Cheng, W. Zhu, Z.-H. Li, Z. Li, X. Ren and Z.-G. Gu, *Dalton Trans.*, 2017, **46**, 8004–8008.
6 V. B. Jakobsen, L. O'Brien, G. Novitchi, H. Müller-Bunz, A. Barra and G. G. Morgan, *Eur. J. Inorg. Chem.*, 2019, 4405–4411.
7 A. Iazzolino, A. Ould Hamouda, A. Naïm, O. Stefánczyk, P. Rosa and E. Freysz, *Appl. Phys. Lett.*, 2017, **110**, 161908.
8 C. Bartual-Murgui, L. Piñeiro-López, F. J. Valverde-Muñoz, M. C. Muñoz, M. Seredyuk and J. A. Real, *Inorg. Chem.*, 2017, **56**, 13535–13546.
9 C. T. Kelly, R. Jordan, S. Felton, H. Müller-Bunz and G. G. Morgan, *Chem. – Eur. J.*, 2023, **29**, e202300275.
10 V. Maliuzhenko, M. Weselski, J. Gregoliński, M. Książek, J. Kusz and R. Bronisz, *Inorg. Chem.*, 2024, **63**, 17762–17773.
11 N. Suryadevara, A. Pausch, E. Moreno-Pineda, A. Mizuno, J. Bürck, A. Baksi, T. Hochdörffer, I. Šalitroš, A. S. Ulrich, M. M. Kappes, V. Schünemann, W. Klopper and M. Ruben, *Chem. – Eur. J.*, 2021, **27**, 15172–15180.
12 X. Zhao, Y. Deng, J. Xi, J. Huang and Y. Zhang, *Angew. Chem.*, 2025, **137**, e202414826.
13 Y. Sekimoto, M. R. Karim, N. Saigo, R. Ohtani, M. Nakamura and S. Hayami, *Eur. J. Inorg. Chem.*, 2017, 1049–1053.
14 N. Shahid, K. E. Burrows, C. M. Pask, O. Cespedes, M. J. Howard, P. C. McGowan and M. A. Halcrow, *Dalton Trans.*, 2022, **51**, 4262–4274.
15 K. E. Burrows, S. E. McGrath, R. Kulmaczewski, O. Cespedes, S. A. Barrett and M. A. Halcrow, *Chem. – Eur. J.*, 2017, **23**, 9067–9075.
16 S. Sundaresan, J.-G. Becker, J. Eppelsheimer, A. E. Sedykh, L. M. Carrella, K. Müller-Buschbaum and E. Rentschler, *Dalton Trans.*, 2023, **52**, 13181–13189.
17 S. Sundaresan, J. Eppelsheimer, E. Gera, L. Wiener, L. M. Carrella, K. R. Vignesh and E. Rentschler, *Dalton Trans.*, 2024, **53**, 10303–10317.
18 S. Sundaresan, J. Eppelsheimer, L. M. Carrella and E. Rentschler, *Eur. J. Inorg. Chem.*, 2025, e202400690.
19 P. N. Basa, C. A. Barr, K. M. Oakley, X. Liang and S. C. Burdette, *J. Am. Chem. Soc.*, 2019, **141**, 12100–12108.
20 H. A. Rajapakse, H. Zhu, M. B. Young and B. T. Mott, *Tetrahedron Lett.*, 2006, **47**, 4827–4830.
21 S. Sundaresan, J. A. Kitchen and S. Brooker, *Inorg. Chem. Front.*, 2020, **7**, 2050–2059.
22 J. K. McCusker, A. L. Rheingold and D. N. Hendrickson, *Inorg. Chem.*, 1996, **35**, 2100–2112.
23 G. S. Matouzenko, A. Bousseksou, S. Lecocq, P. J. Van Koningsbruggen, M. Perrin, O. Kahn and A. Collet, *Inorg. Chem.*, 1997, **36**, 5869–5879.
24 J. Kiehl, T. Hochdörffer, L. M. Carrella, V. Schünemann, M. H. Nygaard, J. Overgaard and E. Rentschler, *Inorg. Chem.*, 2022, **61**, 3141–3151.
25 S. Sundaresan, J. Kiehl, L. M. Carrella and E. Rentschler, *Cryst. Growth Des.*, 2023, **23**, 1648–1655.